
TDDSR: SINGLE-STEP DIFFUSION WITH TWO DISCRIMINATORS FOR SUPER RESOLUTION

Sohwi Kim¹, Tae-Kyun Kim^{1,2}
¹KAIST ²Imperial College London

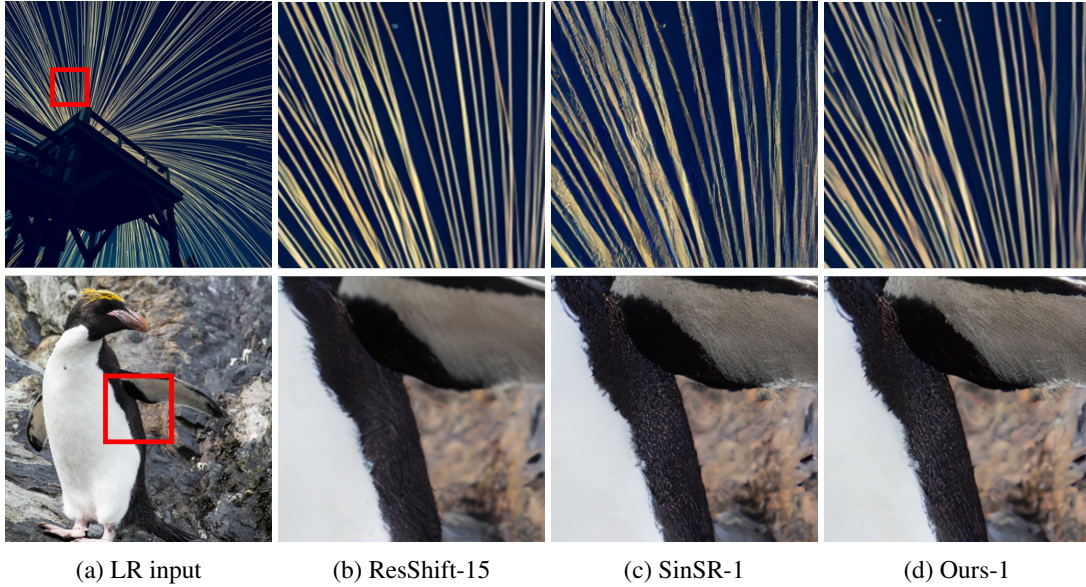


Figure 1: A comparison with the recent state-of-the-art methods, ResShift (multi-step) and SinSR (single-step). Our method performs on par with, or even surpasses, these approaches. The '-N' following each method's name denotes the number of inference steps.

ABSTRACT

Super-resolution methods are increasingly being specialized for both real-world and face-specific tasks. However, many existing approaches rely on simplistic degradation models, which limits their ability to handle complex and unknown degradation patterns effectively. While diffusion-based super-resolution techniques have recently shown impressive results, they are still constrained by the need for numerous inference steps. To address this, we propose TDDSR, an efficient single-step diffusion-based super-resolution method. Our method, distilled from a pre-trained teacher model and based on a diffusion network, performs super-resolution in a single step. It integrates a learnable downsampler to capture diverse degra-

degradation patterns and employs two discriminators—one for high-resolution and one for low-resolution images—to enhance the overall performance. Experimental results demonstrate its effectiveness across real-world and face-specific SR tasks, achieving performance comparable to, or even surpassing, another single-step method, previous state-of-the-art models, and the teacher model.

1 Introduction

The quality of images in real world degrades from various factors, including blurs, compression artifacts, color inaccuracies, and sensor noises. A major challenge in Super-Resolution (SR) is that these diverse degradation patterns are often unknown. Traditionally, degradations have been assumed and modeled using a simple process like Gaus-

sian noise or bicubic downsampling. More sophisticated degradation models [61, 52, 62, 36] have been proposed to reflect real-world conditions better. While these models can be managed effectively, extending their application to unforeseen degradations remains challenging, with complications in achieving realistic image reconstruction.

Meanwhile, in generative tasks using diffusion models, standard diffusion models, despite their efficacy in producing high-quality images and videos, are often limited by their iterative nature, which poses challenges for real-time applications. Although there have been efforts to reduce the number of sampling steps to accelerate the inference, some techniques [37, 46, 29], such as DPM-solver and DDIM, tend to compromise output qualities, often resulting in blurry images. Consequently, ongoing research efforts are dedicated to developing methodologies that improve both the speed and quality of diffusion based generation to facilitate their practical use.

Recent progress in accelerating diffusion sampling has been centered on various distillation techniques to mitigate the limitations, substantially decreasing the number of sampling steps required for diffusion models. Approaches such as Progressive Distillation [42] and Guided Distillation [33] have been introduced to address these challenges. These methods employ a progressive learning strategy, wherein a student model learns to replicate the output of a teacher model in fewer steps, thereby gradually reducing the required steps to just 4-8. This strategy significantly lowers computational costs and accelerates the sampling process [24, 31]. In the context of super-resolution, these distillation techniques facilitate faster and more efficient *training* of diffusion models; however, they often necessitate extensive sampling steps or prolonged training durations, which impede the scalability and adaptability of SR models.

Notable advancements in generative modeling have been made by integrating diffusion models with Generative Adversarial Networks (GANs). This hybrid approach seeks to enhance both the efficiency and output quality of the diffusion process. For example, Denoising Diffusion GANs [58] have been developed to expedite the sampling process, enabling the generation of high-quality images with fewer steps. Subsequent approaches, such as UFOGen [59] and ADD [44], have further explored the integration of discriminators with diffusion models, solidifying this combination as a pivotal method for enhancing performance in generative tasks.

Building upon these developments, we propose a novel approach to Super-Resolution that leverages the strengths of both diffusion models and GANs while considering diverse degradation patterns. Specifically, we introduce a single-step diffusion model for image super-resolution, distilled from a pre-trained diffusion model and augmented by two discriminators. Our methodology involves employing a deterministic sampling strategy and distilling the deterministic generation function [54] into a student network. To further enhance performance, we incorpo-

rate two discriminators: (i) *an HR discriminator*, which utilizes ground-truth high-resolution (HR) images to enhance overall image quality, and (ii) *a Down sampler & LR discriminator*, which uses a flexible downsampler to provide detailed degradation information and compares the generated output with low-resolution (LR) images.

Our contributions are summarized as follows:

- We propose a novel approach combining the diffusion network with two discriminators.
- The method achieves on-par state-of-the-art results with a single-step process.
- Performance is enhanced without increasing the complexity of the student network, keeping the number of parameters constant.
- We demonstrate the excellent performance of the method in real-world SR tasks and on face data.

2 Related Work

2.1 Diffusion model

A diffusion model is a denoising process that starts with noise x_T and gradually produces less noisy samples $x_{T-1}, x_{T-2}, \dots, x_0$. The initial concept of the diffusion model was introduced in [45], where a generative Markov chain is used to gradually transform a known distribution, like a Gaussian, into the target data distribution through a diffusion process. Later, the Denoising Diffusion Probabilistic Model (DDPM) [14], which is now commonly associated with diffusion models, was introduced, demonstrating more effective results. Song et al. [49] mathematically showed that diffusion models can be interpreted as discretized stochastic differential equations (SDEs). The strong theoretical underpinnings of diffusion models have led to remarkable achievements across various domains. In the field of image generation, diffusion models have demonstrated state-of-the-art performance [7, 39]. The versatility and robustness of diffusion models continue to make them a vital area of research in generative modeling.

2.2 Image Super-Resolution

Super-Resolution (SR) is a task that takes a Low-Resolution (LR) image as input and restores a High-Resolution (HR) image by estimating high-frequency details. Since the introduction of the SR task using Deep Neural Networks (DNNs) with SRCNN [8], numerous SR methods based on deep learning have been proposed [38, 56, 39, 41].

Regression-based models [28, 65, 26] focus on learning the mapping between LR and HR images, aiming to generate super-resolved images by minimizing pixel-wise differences. This approach emphasizes accurately restoring the HR image from the LR input. On the other hand, generative-based models take a more creative approach

to producing HR images. Among these, autoregressive-based models [6, 34, 11] have gained increasing attention for their ability to enhance the perceptual quality of generated HR images. These models sequentially generate each part of the image, achieving higher-quality outputs by considering the dependencies between pixels or patches.

GAN-based models. Generative Adversarial Networks (GANs)[10] consists of two competing networks: a generator and a discriminator. The goal of the generator is to synthesize high-resolution images that appear highly realistic, while the discriminator strives to distinguish between real images and those generated by the generator. This adversarial training framework has been effectively employed in the Image Super-Resolution (ISR) task [23, 53, 52, 61, 27, 16]. In particular, GANs have been utilized to achieve realistic ISR, beginning with SRGAN[23], which assumed bicubic downsampling for image degradation. Subsequent research has explored more complex degradation models, such as randomly shuffled and high-order processes, as illustrated by BSRGAN[61] and Real-ESRGAN[52]. These advancements have shown the potential of GAN-based models to handle the complexities of real-world image super-resolution, moving beyond simple degradation models and enhancing the perceptual quality of the generated images.

Diffusion-based models. Recently, diffusion-based models have attracted considerable attention for super-resolution tasks[21, 5, 18, 39, 40, 12]. These approaches generally fall into two main categories: one [39, 40] involves integrating the low-resolution (LR) image directly into the denoising network’s input, while the other [5, 18, 12] leverages prior knowledge of a pre-trained diffusion model. Although these models have shown promising performance, their application is limited due to the extensive number of inference steps needed, which considerably hampers the overall efficiency.

Using Downsampler. When using a learnable downsampler for super-resolution, it typically involves generating low-resolution (LR) images. One approach [3] employs a simple downsampling network to create paired LR-HR images for training with GAN. Another method [1, 51] focuses on learning degradation features or representations to enhance specific tasks. [35] introduces downscaling loss, explicitly penalizing a proposed super-resolved image for deviating from its LR input. Meanwhile, [9] proposes a learnable downsampler that directly influences the upsampler, closely aligning with our approach.

2.3 Accelerating Diffusion Sampling

While diffusion models are capable of generating high-quality outputs, they often suffer from limitations due to the large number of inference steps required. To address this, as mentioned in Sec 1, diffusion sampling can be ac-

celerated through both inference acceleration techniques and distillation methods. Additionally, single-step generative models, such as Consistency Models[48], have been introduced, which enable both distillation and training. This model leverages pre-trained diffusion models and applies self-consistency, offering a promising approach to reducing inference time without sacrificing output quality. Building on this foundation, various studies [20, 30, 47] have explored technical advancements, including research on conditional generation tasks[32]. However, adapting these consistency models for conditional generation tasks, such as super-resolution, remains an area that warrants further investigation.

3 Preliminary

Deterministic sampling. SinSR [54] introduces a non-Markovian reverse process, enabling deterministic sampling and distillation in a single step. In the teacher model ResShift[60], with initial state x_T , the forward process is expressed using the residual, defined as the between the LR and HR images $e_0 = (y - x_0)$ as follows

$$q(x_t | x_0, y) = \mathcal{N}(x_t; x_0 + \eta_t e_0, \kappa^2 \eta_t \mathbf{I}), \quad (1)$$

where y is LR image, x_0 is HR image, κ is a hyperparameter for the noise variance and η_t is a shifting sequence that increases monotonically with the time step t and satisfies $\eta_T \rightarrow 1$ and $\eta_0 \rightarrow 0$. The reverse process is defined as

$$p_\theta(x_{t-1} | x_t, y) = \mathcal{N}\left(x_{t-1} \left| \frac{\eta_{t-1}}{\eta_t} x_t + \frac{\alpha_t}{\eta_t} f_\theta(x_t, y, t), \kappa^2 \frac{\eta_{t-1}}{\eta_t} \alpha_t \mathbf{I} \right.\right), \quad (2)$$

where $\alpha_t = \eta_t - \eta_{t-1}$ for $t > 1$, $\alpha_1 = \eta_1$, and an initial state is $x_T = y + \kappa \sqrt{\eta_T} \epsilon$ where $\epsilon \sim \mathcal{N}(\mathbf{0}, \mathbf{I})$. [54] finds that a non-Markovian reverse process exists and is reformulated as

$$q(x_{t-1} | x_t, x_0, y) = \delta(k_t x_0 + m_t x_t + j_t y), \quad (3)$$

where δ is the unit impulse, and m_t, j_t, k_t are defined with η_t as

$$\begin{cases} m_t = \sqrt{\frac{\eta_{t-1}}{\eta_t}}, \\ j_t = \eta_{t-1} - \sqrt{\eta_{t-1} \eta_t}, \\ k_t = 1 - \eta_{t-1} + \sqrt{\eta_{t-1} \eta_t} - \sqrt{\frac{\eta_{t-1}}{\eta_t}}. \end{cases} \quad (4)$$

Consequently, the reverse process conditioned on a given LR image y is defined as

$$x_{t-1} = k_t \hat{x}_0 + m_t x_t + j_t y, \quad (5)$$

where $\hat{x}_0 = f_\theta(x_t, y, t)$ represents the high-resolution image predicted by a pre-trained teacher model.

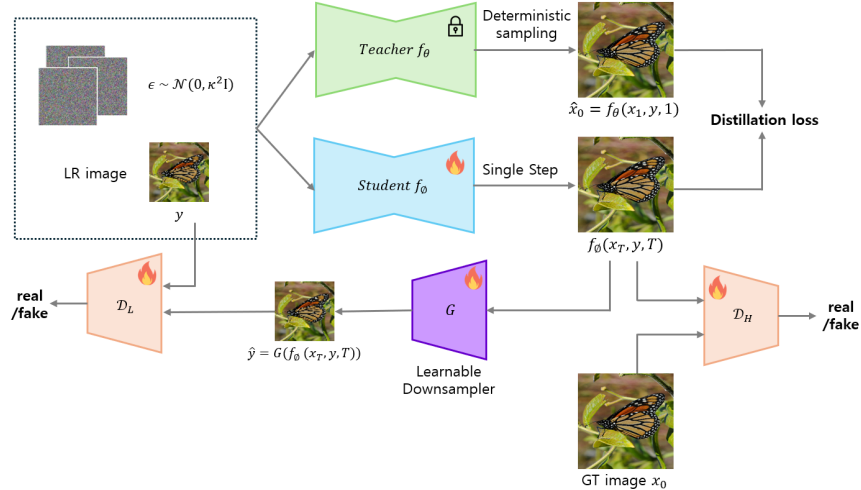


Figure 2: The overall framework of TDDSR. The student network f_ϕ is trained to learn a deterministic mapping from x_T to \hat{x}_0 in just one step, guided by a pre-trained teacher network f_θ . The student’s output $f_\phi(x_T, y, T)$ then goes to the High-Resolution Discriminator \mathcal{D}_H . Simultaneously, $f_\phi(x_T, y, T)$ is also processed by a Learnable Downsampler G and Low-Resolution Discriminator \mathcal{D}_L .

4 Methodology

Our training process, as shown in Fig. 2, involves three paths. The first path focuses on distilling the knowledge from the teacher model into the student model, enabling the Super-Resolution (SR) task to be performed in a single step. The second path involves passing the output $f_\phi(x_T, y, T)$ generated by the student model, along with the ground-truth high-resolution (HR) image, to the HR discriminator, which distinguishes between the two. In the third path, the student’s output $f_\phi(x_T, y, T)$ is processed through a downsampler to estimate a low-resolution image \hat{y} . This estimated image \hat{y} is then compared to the original low-resolution image y by the LR discriminator, which determines whether the image is real or fake. We drew inspiration from DiscoGAN[22] and CycleGAN[66], particularly in their use of cycle consistency loss for bidirectional image translation. These models learn mappings between two domains, x and y , where a function maps x to y , and a reverse function maps y back to x . The cycle consistency loss ensures accurate image reconstruction after both transformations. Similarly, we apply this concept to super-resolution by augmenting the student network, which transforms LR to HR, with a learnable downsampler that performs the HR to LR mapping. Two discriminators compare the generated images with their ground-truths, enforcing consistency and fidelity across both resolutions.

4.1 Distillation

We adapt the concepts of SinSR[54], which are key properties of deterministic mapping, as mentioned in Sec 3. Using the teacher network f_θ and the student network f_ϕ , the teacher model iterates from T down to $t = 1$, as shown

in Eq. 5, we obtain $\hat{x}_0 = f_\theta(x_1, y, 1)$, establishing a deterministic mapping between x_T and \hat{x}_0 . The distillation loss is formulated as

$$\mathcal{L}_{\text{Distill}} = L_{\text{MSE}}(f_\phi(x_T, y, T), \hat{x}_0), \quad (6)$$

where the student network f_ϕ acquires a deterministic mapping from the randomly initialized state x_T to the teacher’s output \hat{x}_0 , distilled to predict the HR image in just *one step*.

4.2 High-Resolution Image discriminator

Need of comparing with GT. In distillation, the student network is trained to perform the super-resolution (SR) task in a single step by minimizing the distillation loss $\mathcal{L}_{\text{Distill}}$, which compares the student’s output to that of the teacher model. However, ground-truth images are not used during this process, with the teacher’s output serving as the target. This limitation affects the student’s performance, as the teacher’s output, while effective, may not fully represent real-world complexities such as diverse degradation patterns. Consequently, the quality of the student network is constrained by the teacher’s output. To mitigate this, we propose using high-resolution ground-truth(GT) images during training to reduce artifacts, improve generalization, and enhance overall image quality.

Inspired by ADD [44], which demonstrated the effectiveness of adversarial loss in image generation, we applied a discriminator in single-step SR distillation to compare the student’s output directly with the high-resolution ground-truth (HR) images.

High-Resolution Image Discriminator. For the discriminator, we adopted the design proposed in StyleGAN-T [43], utilizing and training a feature network. During

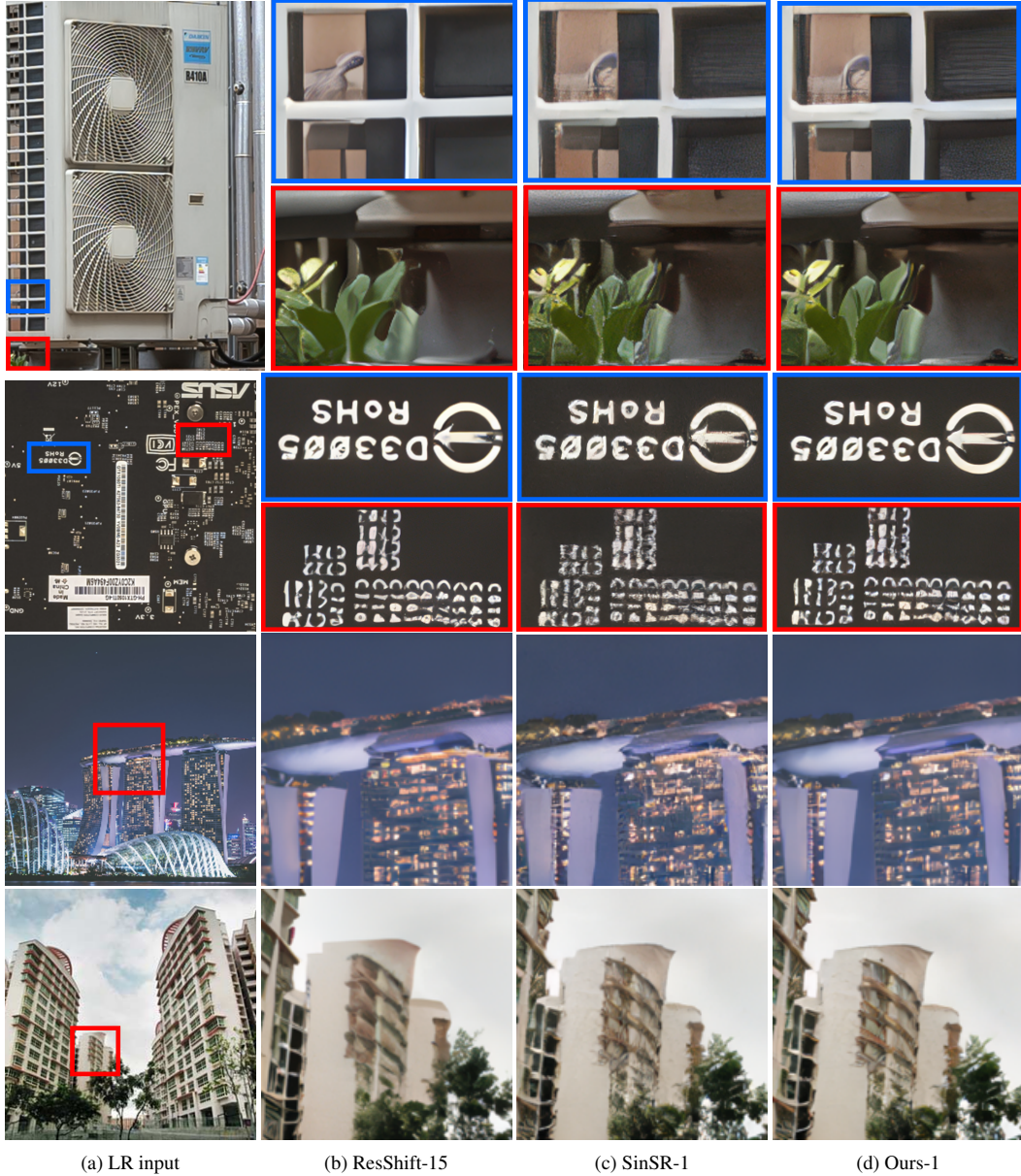


Figure 3: Visual comparisons on real-world super-resolution tasks. Zoom in for more details.

the adversarial training, a high-resolution discriminator \mathcal{D}_H is trained to minimize

$$\mathcal{L}_{\mathcal{D}_H} = \mathbb{E}_{x_0} [\log(1 - \mathcal{D}_H(x_0))] + \mathbb{E}_{f_\phi(x_T, y, T)} [\log(\mathcal{D}_H(f_\phi(x_T, y, T)))], \quad (7)$$

where x_0 is the ground-truth HR image and $f_\phi(x_T, y, T)$ is the student’s predicted high-resolution image. The student network (e.g., the generator) is optimized using the loss function as follows

$$\mathcal{L}_H^G = \mathbb{E}_{f_\phi(x_T, y, T)} [1 - \mathcal{D}_H(f_\phi(x_T, y, T))]. \quad (8)$$

4.3 Learnable Down_sampler and Low-Resolution Image Discriminator

Learnable Down_sampler. The key distinction between prior works and our method lies in its backbone architecture. Leveraging a diffusion network, our approach integrates a flexible down_sampler that spatially adapts the downsampling kernel, enabling it to effectively capture diverse degradation patterns. This design enhances the performance of the diffusion network by providing richer and more varied information during training. The Learnable Down_sampler is composed of convolutional layers designed to dynamically adjust different degradation patterns, offering the adaptability required to address a wide range of image degradation scenarios.

Methods	Datasets			
	RealSR		RealSet65	
	CLIQQA(\uparrow)	MUSIQ(\uparrow)	CLIQQA(\uparrow)	MUSIQ(\uparrow)
RankSRGAN	0.5821	62.0984	0.5600	51.8125
Real-ESRGAN	0.4900	59.6923	0.5987	63.2204
ResShift-15	0.6014	58.6475	0.6489	60.7733
SinSR-1	0.6858	60.7497	0.7146	62.2579
Ours-1	0.7030	61.6313	0.7329	64.5466

Table 1: Quantitative results on the real-world datasets RealSR and RealSet65. The best and second best results of each metric are highlighted in **red** and **blue**.

Methods	Metrics				
	PSNR(\uparrow)	SSIM(\uparrow)	LPIPS(\downarrow)	CLIQQA(\uparrow)	MUSIQ(\uparrow)
RankSRGAN	26.51	0.7526	0.1217	0.6402	64.6863
Real-ESRGAN	26.6511	0.7584	0.2284	0.5645	64.6550
ResShift-15	27.2753	0.7626	0.2005	0.6729	65.5703
SinSR-1	26.6221	0.7319	0.2074	0.7152	65.7644
Ours-1	26.8800	0.7466	0.1977	0.6855	65.8653

Table 2: Quantitative results on DIV2K validation dataset. The best and second best results of each metric are highlighted in **red** and **blue**.

Low-Resolution Image Discriminator. The Low-Resolution Image Discriminator utilizes the same architecture and loss function as described in Sec 4.2. This choice was made to maintain consistency across the model components and to simplify the structural design and implementation process, ensuring a more streamlined and efficient integration within the overall framework.

The low-resolution discriminator \mathcal{D}_L is trained to minimize

$$\mathcal{L}_{\mathcal{D}_L} = \mathbb{E}_y [\log(1 - \mathcal{D}_L(y))] + \mathbb{E}_{\hat{y}} [\log(\mathcal{D}_L(\hat{y}))], \quad (9)$$

where y is the ground-truth low-resolution image, and $\hat{y} = G(f_\phi(x_T, y, T))$ is the LR image predicted by the learnable downsampler G . The downsampler’s adversarial objective amounts to

$$\mathcal{L}_L^G = \mathbb{E}_{\hat{y}} [1 - \mathcal{D}_L(\hat{y})]. \quad (10)$$

5 Experiments

We trained our model using the Adam optimizer with a learning rate of $5e-5$ for 20k iterations. All experiments were conducted on a single NVIDIA A100 GPU with 40GB of memory. Our experiments were performed on both real-world and face datasets, demonstrating the effectiveness of our approach across these domains. To ensure the evaluations are tailored to each task and domain, we used different datasets and metrics for Real Image Super-Resolution (Real-ISR) and Face Super-Resolution (Face-SR). Our investigation specifically targets challenging $\times 4$ times super-resolution tasks. Additionally, we utilized ResShift [60] as the teacher model.

5.1 Real-world Super-Resolution

Datasets. For Real-ISR, we use the DIV2K dataset [2], degraded using the RealESRGAN [52] pipeline, which is consistent with the approach used in SinSR [54]. To gain deeper insights into the generalization performance on unseen real-world data, we also assess our model on RealSR [4] and RealSet65 [60]. The RealSR dataset consists of 100 real images captured using two different cameras, Canon and Nikon, across diverse settings. RealSet65 includes 65 images collected from widely known datasets and online sources.

Metrics and Compared Methods. We evaluate our approach using both reference and non-reference metrics. We use traditional reference metrics such as PSNR and SSIM [55] for fidelity assessment. To evaluate perceptual quality, we employ the LPIPS [63]. Additionally, two recently introduced non-reference metrics, CLIQQA [50] and MUSIQ [19], are used to assess the realism of the generated images. We mainly use CLIQQA and MUSIQ as metrics for evaluating real-world datasets. We compare the performance of TDDSR with several SOTA SR methods, including SinSR [54], ResShift [60], Real-ESRGAN [52], and RankSRGAN [64], to demonstrate its effectiveness.

Results. The results on RealSR and RealSet65 are presented in Table 1. The table demonstrates that the proposed approach outperforms SinSR and the teacher model, even with only a single inference step. In terms of the CLIQQA metric, TDDSR achieves the best performance across both datasets. The results of the DIV2K validation dataset are shown in Table 2. While the PSNR and SSIM values decrease compared to the teacher model due to the reduction in inference steps from 15 to 1,

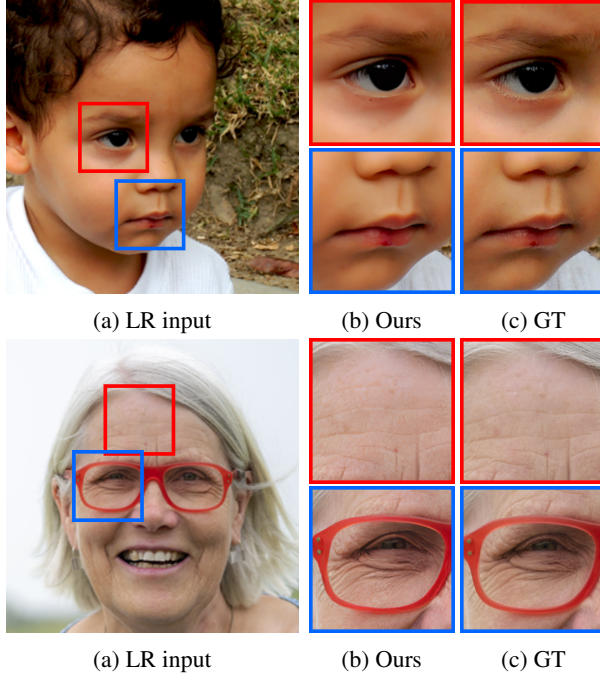


Figure 4: Visual comparison on Face dataset with Low-Resolution inputs and High-Resolution Ground-Truth images. Zoom in for more details.

our one-step model demonstrates superior performance in perceptual quality metrics, including LPIPS and the state-of-the-art metrics CLIPQA and MUSIQ. This indicates that our proposed one-step model performs well from a perceptual and realism perspective. Additionally, compared to SinSR, which also employs a single inference step, our model achieves better performance in all metrics except CLIPQA. Figure 3 presents some visual comparisons among the teacher model ResShift, the single-step model SinSR, and our proposed single-step model. Besides, more comparisons are in the supplementary material.

5.2 Face Super-Resolution

Datasets. For Face Super-Resolution (Face-SR), we utilize the Flickr-Faces-HQ (FFHQ) dataset [17], which contains a diverse collection of 70,000 high-quality human face images. We partition this dataset into non-overlapping subsets: 80% for training, 15% for testing, and 5% for validation.

Metrics and Compared Methods. To quantitatively assess the performance of our face SR methods, we employ a range of evaluation metrics: PSNR, SSIM, Multi-Scale Structural Similarity Index Measure (MS-SSIM) [57], and Fréchet Inception Distance (FID) [13]. These metrics provide a comprehensive evaluation of both image fidelity and perceptual quality. In our comparative analysis, we evaluate our ap-

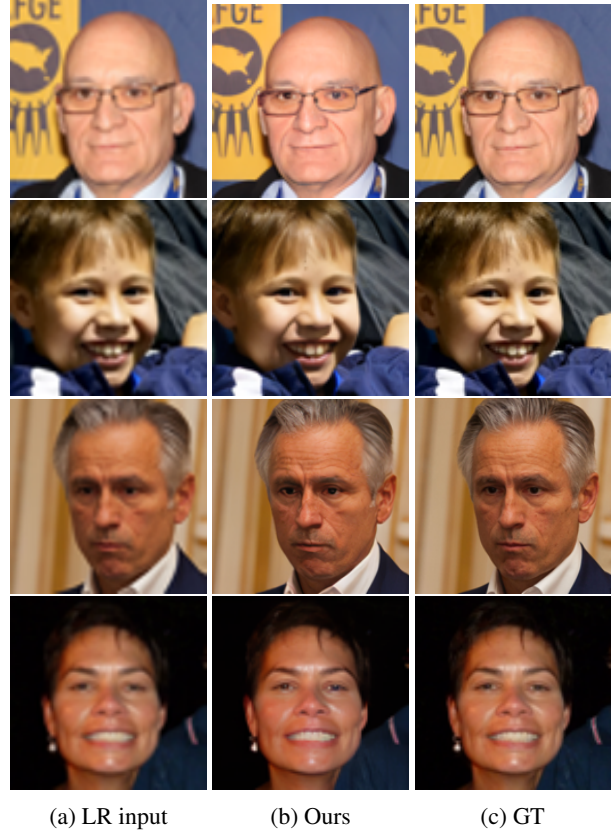


Figure 5: Comparisons of face images with 64×64 inputs upscaled to $4 \times$ high-resolution outputs of 256×256 .

proach against several state-of-the-art methods, including SRGAN [23], ESRGAN [53], EnhanceNet [41], SRFBN [25], CAGFace [15], and SinSR [54]. For a fair comparison, we ensure that all methods are tested under identical experimental settings. Additionally, we compare our results directly with those reported in [15] to provide a clear benchmark against a well-established method.

Results. In Table 4, we present the quantitative results of 64×64 images by $\times 4$ SR, demonstrating that our method achieves superior performance in terms of PSNR, SSIM, and FID metrics compared to other approaches. Qualitative comparisons of the LR input, our SR results, and the ground-truth HR images are provided in Figure 5. We also present the results of 1024×1024 output images in Table 3, where both our method and SinSR used models trained on 256×256 images. Despite this, our method achieves the best performance in terms of FID and ranks second in both PSNR and MS-SSIM. Visual comparisons, depicted in Figure 4, highlight that our method effectively captures fine details such as wrinkles and skin smoothness, closely approximating the quality of GT images. We directly compared our proposed method with the ground-truth to evaluate how closely our results align with the ideal reference images, thus providing a deeper understanding of the perceptual quality and fidelity of our SR

Methods	Metrics			
	PSNR(\uparrow)	SSIM(\uparrow)	MS-SSIM(\uparrow)	FID(\downarrow)
SRGAN	21.49	0.515	0.807	60.67
ESRGAN	19.84	0.353	0.782	72.73
EnhanceNet	29.42	<u>0.832</u>	0.934	19.07
SRFBN	27.90	0.822	0.931	17.14
CAGFace	34.10	0.906	0.971	12.40
SinSR-1	30.91	0.816	0.936	<u>3.633</u>
Ours-1	<u>31.16</u>	0.821	<u>0.937</u>	3.148

Table 3: Quantitative results for 1024×1024 outputs on Face dataset. The best and second best results of each metric are highlighted in red and blue.

Methods	Metric			
	PSNR(\uparrow)	SSIM(\uparrow)	MS-SSIM(\uparrow)	FID(\downarrow)
SRGAN	17.57	0.415	0.757	156.07
ESRGAN	15.43	0.267	0.747	166.36
EnhanceNet	23.64	0.701	0.897	116.38
SRFBN	21.96	0.693	0.895	132.59
CAGFace	27.42	0.816	0.958	74.43
SinSR-1	<u>29.15</u>	<u>0.822</u>	0.952	<u>10.332</u>
Ours-1	29.43	0.829	<u>0.955</u>	9.179

Table 4: Quantitative results for 256×256 outputs on Face dataset. The best and second best results of each metric are highlighted in red and blue.

images. Additionally, further comparisons can be found in the supplementary material.

5.3 Ablation Study

We conducted an ablation study on combining three loss paths, as shown in Table 5. The study compares the following losses: *the distillation loss (Distill)* described in Sec 4.1, *the HR loss* using the student’s SR images with an HR discriminator as explained in Sec 4.2, and *the LR loss* using a learnable downsampler with an LR discriminator, also described in Sec 4.3. We evaluated the performance on real-world datasets, RealSR and RealSet65, using CLIPQA and MUSIQ metrics. The results indicate that all three losses are essential. While combining the distillation loss with either the HR loss or the LR loss improved performance, the best improvement was achieved when all three losses were combined.

Loss	Datasets						
				RealSR		RealSet65	
	Distill	HR	LR	CLIPQA(\uparrow)	MUSIQ(\uparrow)	CLIPQA(\uparrow)	MUSIQ(\uparrow)
O	O	O	0.7030	61.6313	0.7329	64.5466	
O	O	X	0.6909	62.0519	0.7036	<u>64.2709</u>	
O	X	O	0.6887	61.6081	0.7076	63.3870	
O	X	X	0.6221	58.7344	0.6564	60.9495	

Table 5: Ablation Study on real-world datasets. The best and second best results are highlighted in bold and underline.

6 Conclusion

In this work, we introduced a single-step diffusion model equipped with two discriminators to enhance inference efficiency while preserving high generative performance. Our method uniquely updates the student network cyclically, considering both HR and LR perspectives, and integrates an adversarial loss via the discriminators. Additionally, we introduced a learnable downsampler to better capture diverse degradation patterns. We demonstrated the effectiveness of our approach on both Real-ISR and Face-SR tasks. While our method shows improved performance compared to the prior one-step approach, there remain still challenges, particularly with fine-scale details such as very small scene text. We also anticipate that training on larger datasets could further improve the model’s overall generative capabilities.

References

- [1] Andreas Aakerberg, Majed El Helou, Kamal Nasrollahi, and Thomas Moeslund. Pda-rwsr: Pixel-wise degradation adaptive real-world super-resolution. In *Proceedings of the IEEE/CVF Winter Conference on Applications of Computer Vision*, pages 4097–4107, 2024. 3
- [2] Eirikur Agustsson and Radu Timofte. Ntire 2017 challenge on single image super-resolution: Dataset and study. In *Proceedings of the IEEE conference on computer vision and pattern recognition workshops*, pages 126–135, 2017. 6
- [3] Adrian Bulat, Jing Yang, and Georgios Tzimiropoulos. To learn image super-resolution, use a gan to learn how to do image degradation first. In *Proceedings of the European conference on computer vision (ECCV)*, pages 185–200, 2018. 3
- [4] Jianrui Cai, Hui Zeng, Hongwei Yong, Zisheng Cao, and Lei Zhang. Toward real-world single image super-resolution: A new benchmark and a new model. In *Proceedings of the IEEE/CVF international conference on computer vision*, pages 3086–3095, 2019. 6
- [5] Jooyoung Choi, Sungwon Kim, Yonghyun Jeong, Youngjune Gwon, and Sungroh Yoon. Ilvr: Conditioning method for denoising diffusion probabilistic models. *arXiv preprint arXiv:2108.02938*, 2021. 3
- [6] Ryan Dahl, Mohammad Norouzi, and Jonathon Shlens. Pixel recursive super resolution. In *Proceedings of the IEEE international conference on computer vision*, pages 5439–5448, 2017. 3
- [7] Prafulla Dhariwal and Alexander Nichol. Diffusion models beat gans on image synthesis. *Advances in neural information processing systems*, 34:8780–8794, 2021. 2
- [8] Chao Dong, Chen Change Loy, Kaiming He, and Xiaoou Tang. Image super-resolution using deep convolutional networks. *IEEE transactions on pattern analysis and machine intelligence*, 38(2):295–307, 2015. 2
- [9] Stephanie Fu, Mark Hamilton, Laura Brandt, Axel Feldmann, Zhoutong Zhang, and Willian T. Freeman. Featup: A model-agnostic framework for features at any resolution. In *Proceedings of the International Conference on Learning Representations*, 2024. 3

- [10] Ian Goodfellow, Jean Pouget-Abadie, Mehdi Mirza, Bing Xu, David Warde-Farley, Sherjil Ozair, Aaron Courville, and Yoshua Bengio. Generative adversarial nets. *Advances in neural information processing systems*, 27, 2014. 3
- [11] Baisong Guo, Xiaoyun Zhang, Haoning Wu, Yu Wang, Ya Zhang, and Yan-Feng Wang. Lar-sr: A local autoregressive model for image super-resolution. In *Proceedings of the IEEE/CVF Conference on Computer Vision and Pattern Recognition (CVPR)*, pages 1909–1918, 2022. 3
- [12] Lanqing Guo, Yingqing He, Haoxin Chen, Menghan Xia, Xiaodong Cun, Yufei Wang, Siyu Huang, Yong Zhang, Xintao Wang, Qifeng Chen, et al. Make a cheap scaling: A self-cascade diffusion model for higher-resolution adaptation. *arXiv preprint arXiv:2402.10491*, 2024. 3
- [13] Martin Heusel, Hubert Ramsauer, Thomas Unterthiner, Bernhard Nessler, and Sepp Hochreiter. Gans trained by a two time-scale update rule converge to a local nash equilibrium. *Advances in neural information processing systems*, 30, 2017. 7, 12
- [14] Jonathan Ho, Ajay Jain, and Pieter Abbeel. Denoising diffusion probabilistic models. In *Proceedings of Advances in Neural Information Processing Systems*, volume 33, pages 6840–6851, 2020. 2
- [15] Ratheesh Kalarot, Tao Li, and Fatih Porikli. Component attention guided face super-resolution network: Cagface. In *Proceedings of the IEEE/CVF winter conference on applications of computer vision*, pages 370–380, 2020. 7, 12
- [16] Tero Karras, Timo Aila, Samuli Laine, and Jaakko Lehtinen. Progressive growing of gans for improved quality, stability, and variation. In *International Conference on Learning Representations (ICLR)*, 2018. 3
- [17] Tero Karras, Samuli Laine, and Timo Aila. A style-based generator architecture for generative adversarial networks. In *Proceedings of the IEEE/CVF conference on computer vision and pattern recognition*, pages 4401–4410, 2019. 7
- [18] Bahjat Kawar, Michael Elad, Stefano Ermon, and Jiaming Song. Denoising diffusion restoration models. *Advances in Neural Information Processing Systems (NeurIPS)*, 35:23593–23606, 2022. 3
- [19] Junjie Ke, Qifei Wang, Yilin Wang, Peyman Milanfar, and Feng Yang. Musiq: Multi-scale image quality transformer. In *Proceedings of the IEEE/CVF international conference on computer vision*, pages 5148–5157, 2021. 6
- [20] Dongjun Kim, Chieh-Hsin Lai, Wei-Hsiang Liao, Naoki Murata, Yuhta Takida, Toshimitsu Uesaka, Yutong He, Yuki Mitsufuji, and Stefano Ermon. Consistency trajectory models: Learning probability flow ode trajectory of diffusion. *arXiv preprint arXiv:2310.02279*, 2023. 3
- [21] Jinseok Kim and Tae-Kyun Kim. Arbitrary-scale image generation and upsampling using latent diffusion model and implicit neural decoder. In *Proceedings of the IEEE/CVF Conference on Computer Vision and Pattern Recognition*, pages 9202–9211, 2024. 3
- [22] Taeksoo Kim, Moonsu Cha, Hyunsoo Kim, Jung Kwon Lee, and Jiwon Kim. Learning to discover cross-domain relations with generative adversarial networks. In *International conference on machine learning*, pages 1857–1865. PMLR, 2017. 4
- [23] Christian Ledig, Lucas Theis, Ferenc Huszár, Jose Caballero, Andrew Cunningham, Alejandro Acosta, Andrew Aitken, Alykhan Tejani, Johannes Totz, Zehan Wang, et al. Photo-realistic single image super-resolution using a generative adversarial network. In *Proceedings of the IEEE conference on computer vision and pattern recognition*, pages 4681–4690, 2017. 3, 7
- [24] Yanyu Li, Huan Wang, Qing Jin, Ju Hu, Pavlo Chemerys, Yun Fu, Yanzhi Wang, Sergey Tulyakov, and Jian Ren. Snapfusion: Text-to-image diffusion model on mobile devices within two seconds. *Advances in Neural Information Processing Systems*, 36, 2024. 2
- [25] Zhen Li, Jinglei Yang, Zheng Liu, Xiaomin Yang, Gwanggil Jeon, and Wei Wu. Feedback network for image super-resolution. In *Proceedings of the IEEE/CVF conference on computer vision and pattern recognition*, pages 3876–3876, 2019. 7
- [26] Jingyun Liang, Jiezhang Cao, Guolei Sun, Kai Zhang, Luc Van Gool, and Radu Timofte. Swinir: Image restoration using swin transformer. In *Proceedings of the IEEE/CVF International Conference on Computer Vision (ICCV)*, pages 1833–1844, 2021. 2
- [27] Jie Liang, Hui Zeng, and Lei Zhang. Details or artifacts: A locally discriminative learning approach to realistic image super-resolution. In *Proceedings of the IEEE/CVF Conference on Computer Vision and Pattern Recognition (CVPR)*, pages 5657–5666, 2022. 3
- [28] Bee Lim, Sanghyun Son, Heewon Kim, Seungjun Nah, and Kyoung Mu Lee. Enhanced deep residual networks for single image super-resolution. In *Proceedings of CVPR Workshops (CVPRW)*, 2017. 2
- [29] Cheng Lu, Yuhao Zhou, Fan Bao, Jianfei Chen, Chongxuan Li, and Jun Zhu. Dpm-solver: A fast ode solver for diffusion probabilistic model sampling in around 10 steps. *Advances in Neural Information Processing Systems*, 35:5775–5787, 2022. 2
- [30] Haoye Lu, Yiwei Lu, Dihong Jiang, Spencer Ryan Szabados, Sun Sun, and Yaoliang Yu. Cm-gan: Stabilizing gan training with consistency models. In *ICML 2023 Workshop on Structured Probabilistic Inference* & *Generative Modeling*, 2023. 3
- [31] Eric Luhman and Troy Luhman. Knowledge distillation in iterative generative models for improved sampling speed. *arXiv preprint*, arXiv:2101.02388, 2021. 2
- [32] Kangfu Mei, Mauricio Delbracio, Hossein Talebi, Zhengzhong Tu, Vishal M Patel, and Peyman Milanfar. Codi: Conditional diffusion distillation for higher-fidelity and faster image generation. In *Proceedings of the IEEE/CVF Conference on Computer Vision and Pattern Recognition*, pages 9048–9058, 2024. 3
- [33] Chenlin Meng, Robin Rombach, Ruiqi Gao, Diederik Kingma, Stefano Ermon, Jonathan Ho, and Tim Salimans. On distillation of guided diffusion models. In *Proceedings of the IEEE/CVF Conference on Computer Vision and Pattern Recognition (CVPR)*, pages 14297–14306, 2023. 2
- [34] Jacob Menick and Nal Kalchbrenner. Generating high fidelity images with subscale pixel networks and multi-dimensional upscaling. In *International Conference on Learning Representations (ICLR)*, 2018. 3
- [35] Sachit Menon, Alexandru Damian, Shijia Hu, Nikhil Ravi, and Cynthia Rudin. Pulse: Self-supervised photo upsampling via latent space exploration of generative models. In *Proceedings of the IEEE/CVF conference on computer vision and pattern recognition*, pages 2437–2445, 2020. 3
- [36] Chong Mou, Yanze Wu, Xintao Wang, Chao Dong, Jian Zhang, and Ying Shan. Metric learning based interactive modulation for real-world super-resolution. In *Proceedings of the European Conference on Computer Vision (ECCV)*, pages 723–740, 2022. 2

- [37] Alexander Quinn Nichol and Prafulla Dhariwal. Improved denoising diffusion probabilistic models. In *Proceedings of the International Conference on Machine Learning (ICML)*, pages 8162–8171. PMLR, 2021. 2
- [38] Niki Parmar, Ashish Vaswani, Jakob Uszkoreit, Lukasz Kaiser, Noam Shazeer, Alexander Ku, and Dustin Tran. Image transformer. In *International conference on machine learning*, pages 4055–4064. PMLR, 2018. 2
- [39] Robin Rombach, Andreas Blattmann, Dominik Lorenz, Patrick Esser, and Björn Ommer. High-resolution image synthesis with latent diffusion models. In *Proceedings of the IEEE/CVF Conference on Computer Vision and Pattern Recognition (CVPR)*, pages 10684–10695, 2022. 2, 3
- [40] Chitwan Saharia, Jonathan Ho, William Chan, Tim Salimans, David J. Fleet, and Mohammad Norouzi. Image super resolution via iterative refinement. *IEEE Transactions on Pattern Analysis and Machine Intelligence (TPAMI)*, 45(4):4713–4726, 2022. 3
- [41] Mehdi SM Sajjadi, Bernhard Scholkopf, and Michael Hirsch. Enhancenet: Single image super-resolution through automated texture synthesis. In *Proceedings of the IEEE international conference on computer vision*, pages 4491–4500, 2017. 2, 7
- [42] Tim Salimans and Jonathan Ho. Progressive distillation for fast sampling of diffusion models. *arXiv preprint arXiv:2202.00512*, 2022. 2
- [43] Axel Sauer, Tero Karras, Samuli Laine, Andreas Geiger, and Timo Aila. Stylegan-t: Unlocking the power of gans for fast large-scale text-to-image synthesis. In *International conference on machine learning*, pages 30105–30118. PMLR, 2023. 4
- [44] Axel Sauer, Dominik Lorenz, Andreas Blattmann, and Robin Rombach. Adversarial diffusion distillation. *arXiv preprint arXiv:2311.17042*, 2023. 2, 4
- [45] Jascha Sohl-Dickstein, Eric Weiss, Niru Maheswaranathan, and Surya Ganguli. Deep unsupervised learning using nonequilibrium thermodynamics. In *International Conference on Machine Learning (ICML)*, pages 2256–2265. PMLR, 2015. 2
- [46] Jiaming Song, Chenlin Meng, and Stefano Ermon. Denoising diffusion implicit models. In *Proceedings of the International Conference on Learning Representations (ICLR)*, 2021. 2
- [47] Yang Song and Prafulla Dhariwal. Improved techniques for training consistency models. *arXiv preprint arXiv:2310.14189*, 2023. 3
- [48] Yang Song, Prafulla Dhariwal, Mark Chen, and Ilya Sutskever. Consistency models. In *Proceedings of the International Conference on Machine Learning (ICML)*, 2023. 3
- [49] Yang Song, Jascha Sohl-Dickstein, Diederik P Kingma, Abhishek Kumar, Stefano Ermon, and Ben Poole. Score-based generative modeling through stochastic differential equations. In *Proceedings of International Conference on Learning Representations (ICLR)*, 2021. 2
- [50] Jianyi Wang, Kelvin CK Chan, and Chen Change Loy. Exploring clip for assessing the look and feel of images. In *Proceedings of the AAAI Conference on Artificial Intelligence*, pages 2555–2563, 2023. 6
- [51] Tao Wang, Kaihao Zhang, Ziqian Shao, Wenhan Luo, Bjorn Stenger, Tae-Kyun Kim, Wei Liu, and Hongdong Li. Lldiffusion: Learning degradation representations in diffusion models for low-light image enhancement. *arXiv preprint arXiv:2307.14659*, 2023. 3
- [52] Xintao Wang, Liangbin Xie, Chao Dong, and Ying Shan. Real-esrgan: Training real-world blind super-resolution with pure synthetic data. In *Proceedings of the IEEE/CVF International Conference on Computer Vision (ICCV)*, pages 1905–1914, 2021. 2, 3, 6
- [53] Xintao Wang, Ke Yu, Shixiang Wu, Jinjin Gu, Yihao Liu, Chao Dong, Yu Qiao, and Chen Change Loy. Esrgan: Enhanced super-resolution generative adversarial networks. In *Proceedings of the European conference on computer vision (ECCV) workshops*, pages 0–0, 2018. 3, 7
- [54] Yufei Wang, Wenhan Yang, Xinyuan Chen, Yaohui Wang, Lanqing Guo, Lap-Pui Chau, Ziwei Liu, Yu Qiao, Alex C Kot, and Bihan Wen. Sinsr: diffusion-based image super-resolution in a single step. In *Proceedings of the IEEE/CVF Conference on Computer Vision and Pattern Recognition*, pages 25796–25805, 2024. 2, 3, 4, 6, 7, 12
- [55] Zhou Wang, Alan C Bovik, Hamid R Sheikh, and Eero P Simoncelli. Image quality assessment: from error visibility to structural similarity. *IEEE transactions on image processing*, 13(4):600–612, 2004. 6
- [56] Zhihao Wang, Jian Chen, and Steven CH Hoi. Deep learning for image super-resolution: A survey. *IEEE transactions on pattern analysis and machine intelligence*, 43(10):3365–3387, 2020. 2
- [57] Zhou Wang, Eero P Simoncelli, and Alan C Bovik. Multi-scale structural similarity for image quality assessment. In *The Thirty-Seventh Asilomar Conference on Signals, Systems & Computers, 2003*, volume 2, pages 1398–1402. Ieee, 2003. 7
- [58] Zhisheng Xiao, Karsten Kreis, and Arash Vahdat. Tackling the generative learning trilemma with denoising diffusion gans. In *International Conference on Learning Representations (ICLR)*, 2022. 2
- [59] Yanwu Xu, Yang Zhao, Zhisheng Xiao, and Tingbo Hou. Ufogen: You forward once large scale text-to-image generation via diffusion gans. In *Proceedings of the IEEE/CVF Conference on Computer Vision and Pattern Recognition (CVPR)*, pages 8196–8206, 2024. 2
- [60] Zongsheng Yue, Jianyi Wang, and Chen Change Loy. Resshift: Efficient diffusion model for image super-resolution by residual shifting. In *Proceedings of Advances in Neural Information Processing Systems (NeurIPS)*, 2023. 3, 6, 12
- [61] Kai Zhang, Jie Liang, Luc Van Gool, and Radu Timofte. Designing a practical degradation model for deep blind image super-resolution. In *Proceedings of the IEEE/CVF International Conference on Computer Vision (ICCV)*, pages 4791–4800, 2021. 2, 3
- [62] Kai Zhang, Wangmeng Zuo, and Lei Zhang. Learning a single convolutional super-resolution network for multiple degradations. In *Proceedings of the IEEE/CVF Conference on Computer Vision and Pattern Recognition (CVPR)*, pages 3262–3271, 2018. 2
- [63] Richard Zhang, Phillip Isola, Alexei A Efros, Eli Shechtman, and Oliver Wang. The unreasonable effectiveness of deep features as a perceptual metric. In *Proceedings of the IEEE conference on computer vision and pattern recognition*, pages 586–595, 2018. 6
- [64] Wenlong Zhang, Yihao Liu, Chao Dong, and Yu Qiao. Ranksrgan: Generative adversarial networks with ranker for image super-resolution. In *Proceedings of the*

- IEEE/CVF international conference on computer vision*, pages 3096–3105, 2019. 6
- [65] Yulun Zhang, Kunpeng Li, Kai Li, Lichen Wang, Bineng Zhong, and Yun Fu. Image super-resolution using very deep residual channel attention networks. In *Proceedings of the European Conference on Computer Vision (ECCV)*, 2018. 2
- [66] Jun-Yan Zhu, Taesung Park, Phillip Isola, and Alexei A Efros. Unpaired image-to-image translation using cycle-consistent adversarial networks. In *Proceedings of the IEEE international conference on computer vision*, pages 2223–2232, 2017. 4

Supplementary Material

In this Supplementary Material, we provide additional qualitative results for both real-world and facial datasets, as well as further ablation studies.

S.1. Experiment Details

Similar to the main paper, we present experimental results for both Real-World Super-Resolution and Face Super-Resolution, along with visual comparisons of the outcomes. Fig 6 illustrates the results of $4\times$ super-resolution on real-world datasets, comparing our method to ResShift (multi-step) [60] and SinSR (single-step) [54]. Fig 7 and Fig 8 provide detailed comparisons for face datasets with 1024×1024 output resolutions. Our model was trained on ground truth images of size 256, and while the current results are promising relative to the ground truth—demonstrating the scalability of the model—we believe that training the model with 1024×1024 ground truth data could further enhance both quantitative and qualitative performance. The comparisons are highlighted by observing the boxed areas in the low-resolution (LR) input, where the colored boxes correspond to our results and the ground truth. Fig 9 and Fig 10 show comparisons using a 64×64 input and a 256×256 output. Furthermore, when calculating the FID [13] score, we used the Inception-v3 pool3 layer to ensure consistency with the models and results reported in previous studies [15].

S.2. Ablation Study

Three Losses. In the main paper, we conducted an ablation study on three losses: Distillation loss, HR loss (using an HR discriminator), and LR loss (using a learnable downsampler and LR discriminator). From a visual perspective, as shown in Fig 11, when zoomed in for detailed inspection, there is a noticeable difference, the combination of all three losses helping to reduce artifacts.

Pretrained Discriminators. We also conducted an ablation study to compare the results with and without pre-training the two discriminators. The HR discriminator was pre-trained using fake images generated by the Teacher model, ResShift [60]. For the LR discriminator, we employed a learnable downsampler to generate fake LR images by training on both HR and LR ground-truth images.

The results, based on experiments using the DIV2K validation dataset, are presented in Table 6. In these experiments, v1 corresponds to the model without pre-trained discriminators, while v2 corresponds to the model with pre-trained discriminators. The use of pre-trained discriminators yields better performance on the CLIPQA and MUSIQ metrics. However, for PSNR, SSIM, and

LPIPS, the model without pre-trained discriminators produces better results. Given that the differences in performance are not substantial, we chose not to pre-train the discriminators in this study.

Methods	Metrics				
	PSNR(\uparrow)	SSIM(\uparrow)	LPIPS(\downarrow)	CLIPQA(\uparrow)	MUSIQ(\uparrow)
Ours v1	26.8800	0.7466	0.1977	0.6855	65.8653
Ours v2	26.8058	0.7413	0.2023	0.6971	66.5178

Table 6: Ablation study comparing the results with and without pretraining the two discriminators

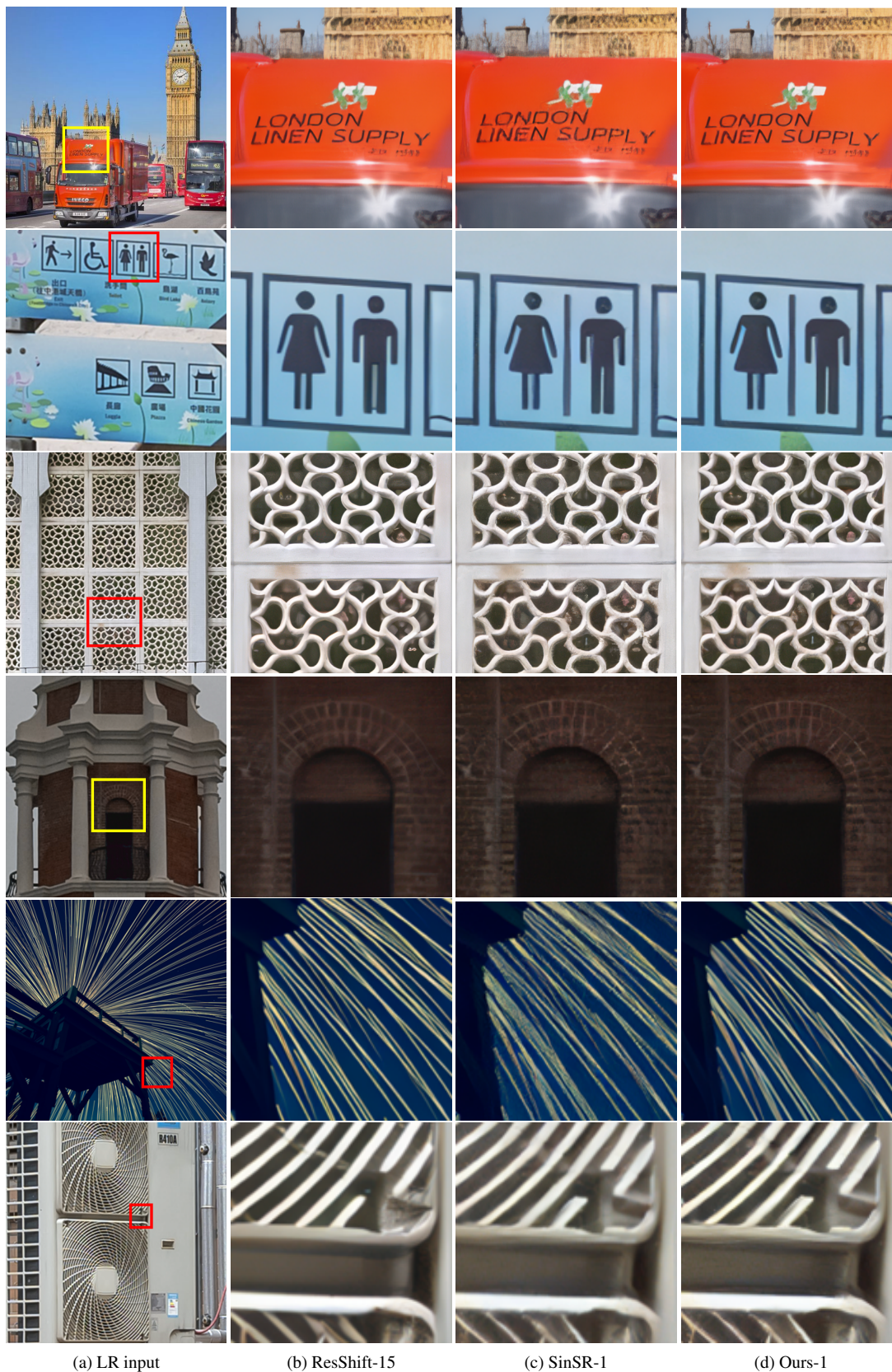


Figure 6: Visual comparisons on real-world super-resolution tasks. Zoom in for more details.

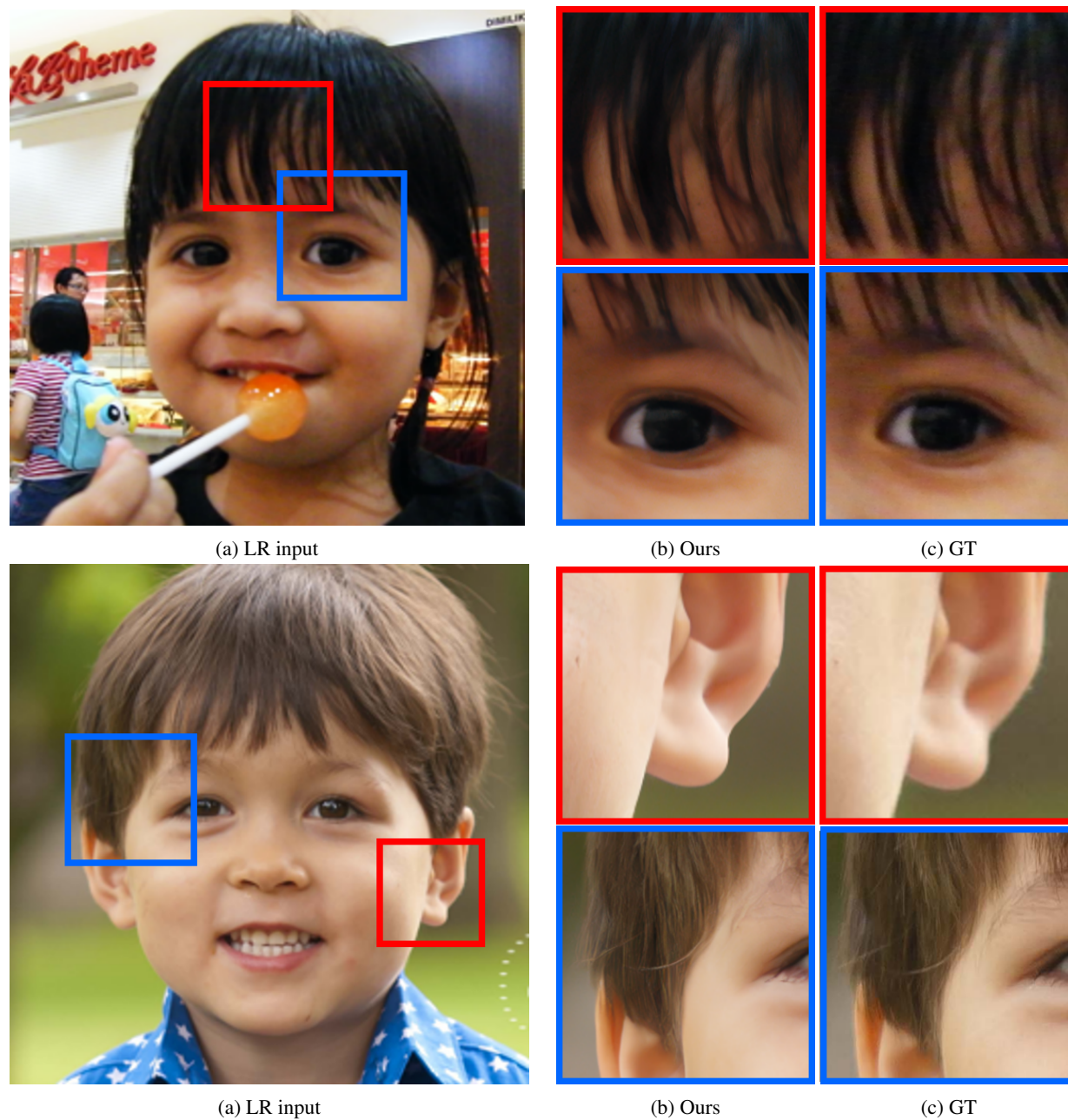


Figure 7: Visual comparison on Face dataset with Low-Resolution inputs and High-Resolution Ground-Truth images. Zoom in for more details.

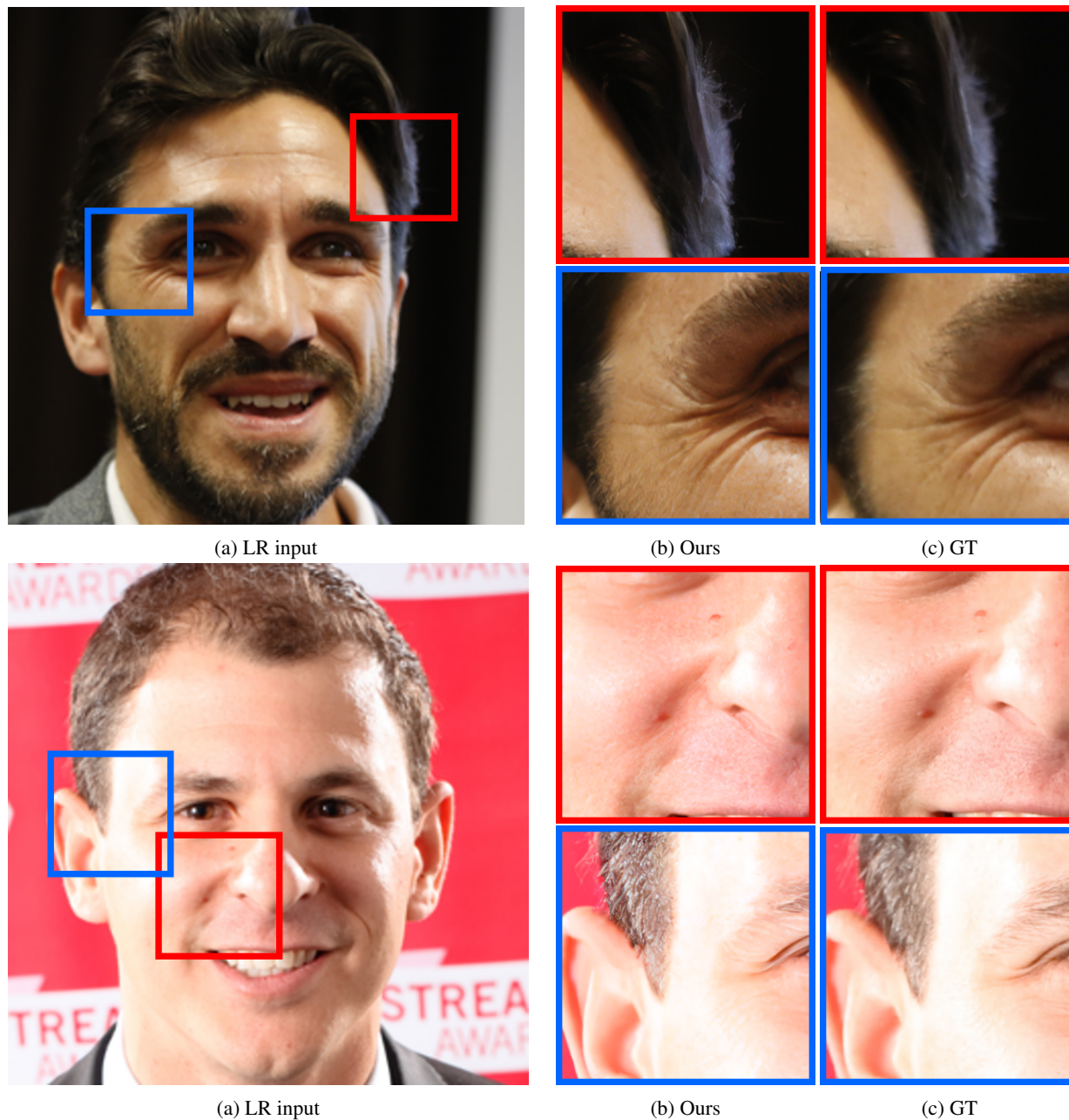


Figure 8: Visual comparison on Face dataset with Low-Resolution inputs and High-Resolution Ground-Truth images. Zoom in for more details.

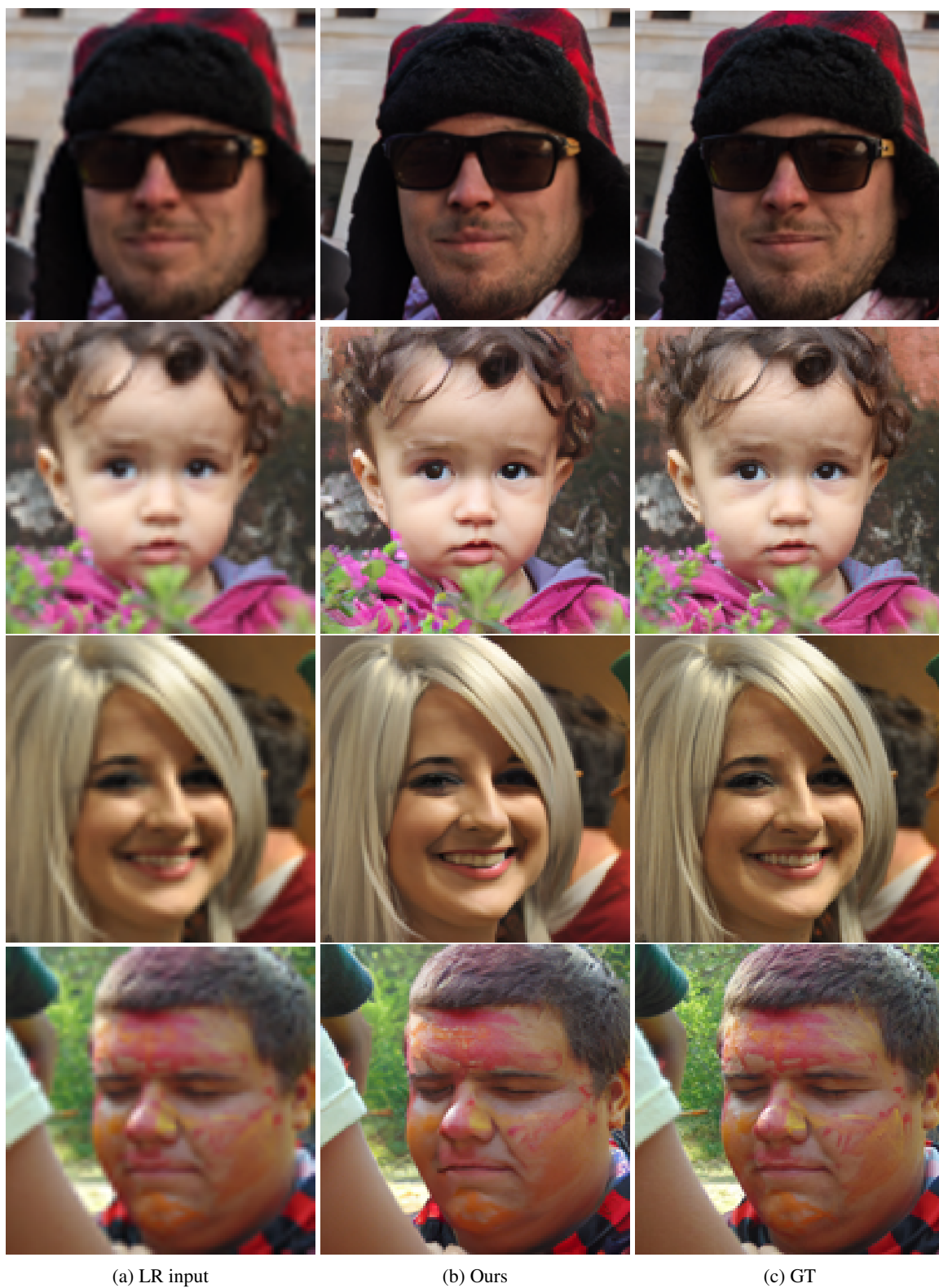


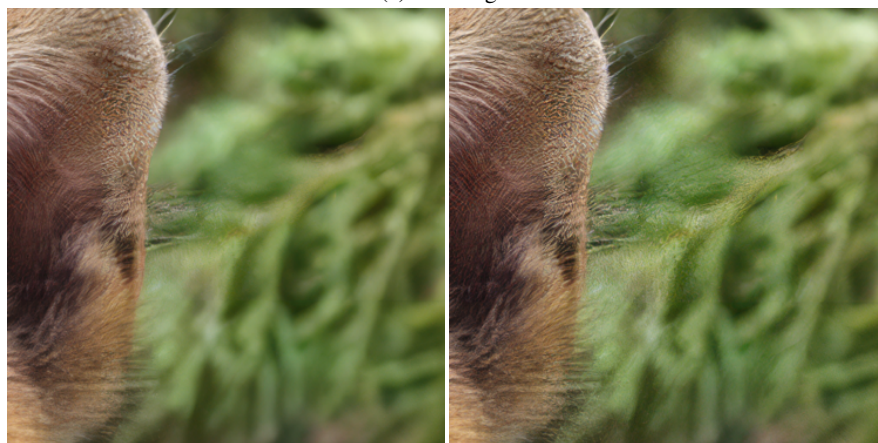
Figure 9: Comparisons of face images with 64×64 inputs upscaled to $4 \times$ high-resolution outputs of 256×256 .



Figure 10: Comparisons of face images with 64×64 inputs upscaled to $4 \times$ high-resolution outputs of 256×256 .

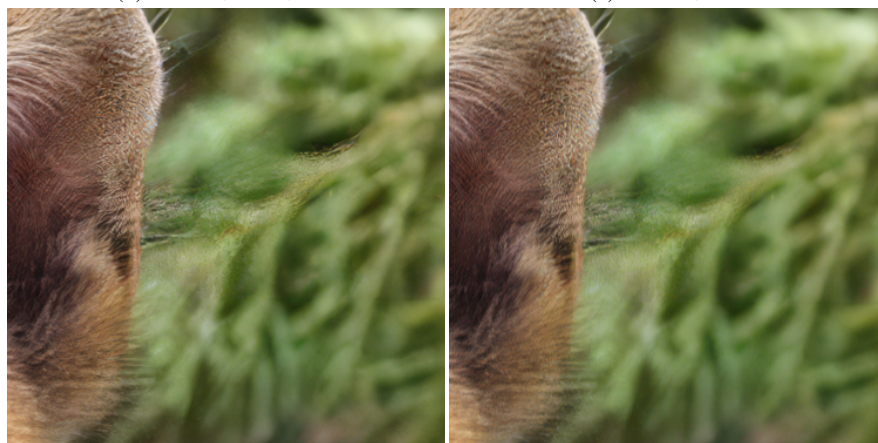


(a) LR image



(b) Distill + HR + LR

(c) Distill + HR



(d) Distill + LR

(e) Distill

Figure 11: Visual comparisons for the ablation study on the combination of three losses.